Seasonal cycles of O_3, CO, and convective outflow at the tropical tropopause

Ian Folkins,[1] P. Bernath,[2] C. Boone,[2] G. Lesins,[1] N. Livesey,[3] A. M. Thompson,[4] K. Walker,[2] and J. C. Witte[5]

[1] Measurements from the SHADOZ ozonesonde network and Aura MLS are used to show that there are seasonal cycles in ozone (O_3) and carbon monoxide (CO) at the tropical tropopause ($\sim$17 km). A simple model, driven by cloud free radiative mass fluxes, is used to investigate the origin of these seasonal cycles. The seasonal cycle in O_3 is due to seasonal changes in upwelling and high altitude convective outflow. The seasonal cycle in CO at 100 hPa is influenced by both seasonal changes in dynamics and seasonal changes in CO at lower altitudes. The age of air at 17 km varies from 40 days during NH winter to 70 days during NH summer. The seasonal cycle in clear sky radiative heating at the tropical tropopause is mainly due to seasonal cycles in O_3 and temperature. The seasonal cycle in O_3 can be expected to amplify the seasonal cycle in cold point temperature. **Citation:** Folkins, I., P. Bernath, C. Boone, G. Lesins, N. Livesey, A. M. Thompson, K. Walker, and J. C. Witte (2006), Seasonal cycles of O_3, CO, and convective outflow at the tropical tropopause, *Geophys. Res. Lett.*, *33*, L16802, doi:10.1029/2006GL026602.

1. Introduction

[2] In the tropics, very high clouds with cloud top temperatures less than 200 K are observed more frequently during Northern Hemisphere (NH) winter than summer [*Zhang*, 1993]. One would expect an increased incidence of very high clouds to be associated with an increased incidence of high altitude convective outflow. A seasonal cycle in convective outflow should give rise to seasonal cycles in convectively influenced trace gas species. There is a significant seasonal cycle in ozone (O_3) at the tropical tropopause, both in the tropical mean [*Randel et al.*, 2006], as well as at individual locations [*Logan*, 1999; *Thompson et al.*, 2003b]. Here, we show that there is also a seasonal cycle in carbon monoxide (CO) at the tropical tropopause ($\sim$17 km), and that the seasonal cycles of O_3 and CO can be approximately reproduced with a simple two column model.

We also obtain an estimate for the seasonal variation of age of air at 17 km.

2. Seasonal Variation of Convective Outflow

[3] Figure 1 (right) shows the vertical variation of tropical mean clear sky radiative mass flux between 14.5 and 17.2 km, for the months of February, May, August, and November. The clear sky radiative mass flux ω_r can be expressed as $\omega_r = -Q_r/\sigma$, where Q_r is the clear sky radiative heating rate and σ is the static stability. Monthly mean estimates of Q_r were calculated using a radiative transfer model [*Fu and Liou*, 1992]. This was done at 10 ozonesonde stations from the SHADOZ network (Southern Hemisphere Additional Ozonesonde ozonesonde stations [*Thompson et al.*, 2003a, 2003b]), and 12 radiosonde stations from the SPARC network (Stratospheric Processes and their Role in Climate). Each station was between 20°S and 20°N. The relative humidity at each site was specified from sonde measurements below 10 km, by a tropical mean aircraft climatology between 12.5 and 16 km [*Folkins and Martin*, 2005], and interpolated between 10 and 12.5 km. Above 17 km, the water vapor mixing ratio was specified by a zonal mean monthly climatology from the Halogen Occultation Experiment (HALOE) instrument [*Grooss and Russell*, 2005]. At the SPARC sites, the O_3 profiles were set equal to the O_3 profile of the SHADOZ site with the nearest latitude, or a monthly mean O_3 profile from Hilo (available from the World Ozone and Ultraviolet Radiation Data Centre, www.woudc.org). To generate the tropical mean ω_r profiles shown in Figure 1, the ω_r profiles of the various stations were grouped into 10 degree intervals, and averaged together.

[4] We will assume that the tropics can be usefully divided into a clear sky column and a cloudy column. To the extent that mass exchange with the extratropics can be neglected [*Folkins and Martin*, 2005], the net rate at which air flows inward or outward from the cloudy column (δ_c) must be balanced by a radiative mass flux divergence (δ_r) of the clear sky column. If ω_r and ω_c refer to the tropical mean mass fluxes of the clear sky and cloudy columns, then

$$\delta_c + \delta_r = \frac{\partial \omega_c}{\partial p} + \frac{\partial \omega_r}{\partial p} = 0. \tag{1}$$

This equation can be used to calculate the cloud divergence (δ_c) from the tropical mean ω_r profile. The cloud divergence is the sum of two processes: detrainment of cloudy air into the clear sky column and entrainment of clear sky air into the cloudy column. In the upper troposphere, it is likely that detrainment (d) dominates entrainment, in which case

[1]Department of Physics and Atmospheric Science, Dalhousie University, Halifax, Nova Scotia, Canada.
[2]Department of Chemistry, University of Waterloo, Waterloo, Ontario, Canada.
[3]Jet Propulsion Laboratory, Pasadena, California, USA.
[4]Department of Meteorology, Penn State University, University Park, Pennsylvania, USA.
[5]Science Systems and Applications, Inc., NASA Goddard Space Flight Center, Greenbelt, Maryland, USA.
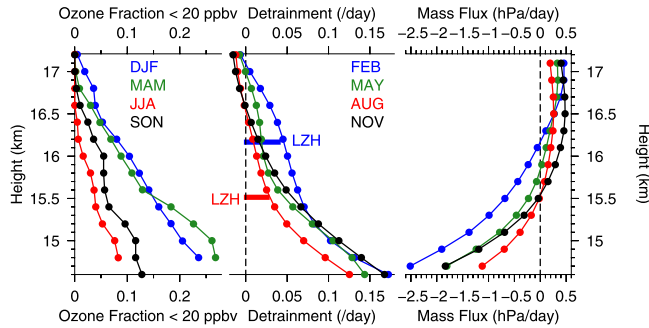
Figure 1. (left) Fraction of ozone measurements less than 20 ppbv, averaged over the SHADOZ sites Watukosek (Java), Samoa, and Fiji, for the seasons shown. (middle) Monthly tropical mean (20°S−20°N) rate of convective detrainment for various months, as diagnosed from clear sky radiative heating rates. The horizontal bars indicate the Level of Zero radiative Heating (LZH) for August and February. (right) Tropical mean clear sky radiative mass flux ω_r. (For clarity, we have used a convention in which a positive ω_r refers to an upward mass flux).

$d \approx \delta_c$. Figure 1 (middle) shows the tropical mean cloud detrainment profiles corresponding to the ω_r profiles shown in Figure 1 (right), under this assumption. Convective outflow is quite weak above 14.5 km. (A detrainment rate $d = 0.05$ day^{-1} indicates that deep convection replaces air in the 20°S−20°N interval at that altitude on average once every 20 days.) Above 15.5 km, deep convective outflow in January is significantly stronger than in the other three months, and persists to a higher altitude.

[5] At maritime locations characterized by persistent deep convection, the fraction of air parcels with O₃ mixing ratios less than 20 ppbv has been used as a proxy for the frequency of convective outflow [*Folkins et al.*, 2002; *Solomon et al.*, 2005; *Folkins et al.*, 2006]. Figure 1 (left) shows the likelihood of observing an air parcel with [O₃] < 20 ppbv, averaged over three SHADOZ ozonesonde locations: Watukosek (Java), Samoa, and Fiji. For each season, the height at which the O₃ fraction goes to zero closely approximates the height at which the convective detrainment of the corresponding month goes to zero.

3. Seasonal Variation of Ozone and Carbon Monoxide

[6] The profiles of radiative mass flux and detrainment shown in Figure 1 can be used as inputs into an equation which solves for the mean tropical profile [X] of a trace species [*Folkins and Martin*, 2005].

$$\frac{\partial [X]}{\partial t} = -\omega_r \frac{\partial [X]}{\partial p} + P - L[X] + d\big([X]_{\text{conv}} - [X]\big) \quad (2)$$

[X]$_{\text{conv}}$ is the mean mixing ratio of the species in convective outflow. P is the rate of production of [X], and L is the loss rate. The first term on the right hand side of (2) represents the tendency due to vertical advection, the second and third terms the tendency due to *in situ* chemistry, and the fourth term the tendency due to convective outflow. [X]$_{\text{conv}}$ is the only free parameter of the model, and for insoluble species,

should roughly equal the mean mixing ratio of the species in the boundary layer. In the region of interest, estimates for P and L for both O₃ and CO were determined from measurements of OH, HO₂, NO, and calculations of O₂ photolysis, from aircraft measurements [*Folkins et al.*, 2006]. The model assumes that sources of clear sky mixing (such as wave breaking, or stochastic variations in cloud free radiative heating rates) can be neglected, but that horizontal transport is sufficiently fast that the effects of horizontal inhomogeneities on the calculated mean profiles are not significant.

[7] The solid black curve in Figure 2 shows the seasonal variation of tropical mean O₃ at 17 km obtained from the SHADOZ measurements. The solid blue curve represents the seasonal variation of O₃ predicted by (2) using [O₃]$_{\text{conv}}$ = 30 ppbv. The model tends to overpredict O₃ during NH summer, but is otherwise quite successful at reproducing the seasonal cycle of O₃ at 17 km.

[8] Figure 2 also shows that the amplitude of the seasonal cycle in tropical mean O₃ increases dramatically in going from 14 km to 17 km. This increase in amplitude is roughly captured by a model in which there is no seasonal variation in O₃ production or loss. It therefore seems likely that the increase in amplitude is mainly driven by some combination of seasonal changes in convective outflow and upwelling.

[9] Figure 1 shows the convective detrainment rate d is sometimes negative below 17 km. In these cases, we set $d = 0$ when using (2) to solve for the O₃ profile. However, negative values of convective detrainment do not arise below 17 km when one takes mass exchange with the extratropics into account. We used temperatures and meridional winds from the ERA - 40 reanalysis to calculate the export of mass across the 20°S and 20°N latitude circles for each month of 2000. We then adjusted the monthly mean
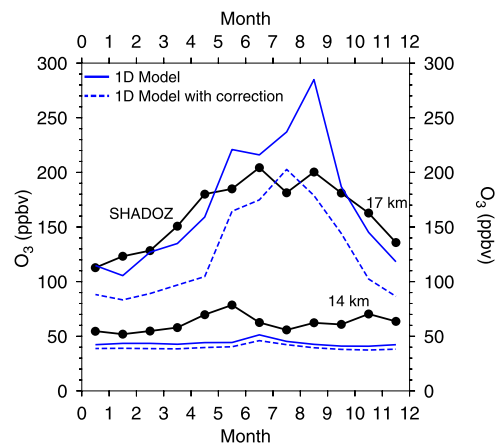

Figure 2. The upper black line shows the seasonal cycle of tropical mean ozone (20°S−20°N) at 17 km. It was obtained by averaging over the 11 SHADOZ ozonesonde stations within this latitudinal band, and Hilo (19.7°N). The lower black line shows the seasonal cycle of tropical mean ozone at 14 km. The solid blue lines show the seasonal cycles of tropical mean ozone at 14 km and 17 km generated by the one-dimensional model. The dashed blue lines refer to a version of the model in which convective outflow in the upper tropical troposphere is increased by an amount equal to the export of mass outside the 20°S−20°N latitude band.

convective detrainment profiles upward by an equal amount to compensate for this net mass export. The dashed curves in Figure 1 show the O_3 seasonal cycles calculated with this correction. The increase in convective outflow reduces upper tropospheric O_3 by a proportionally greater amount at higher altitudes. The correction increases agreement with SHADOZ O_3 during NH summer, but diminishes agreement during NH winter.

[10] The existence of a mass export from the tropics to the extratropics in the vicinity of the tropical tropopause is supported by cloud radiative heating calculations [*Corti et al.*, 2005], as well as by calculations using winds from other analyses [*Folkins and Martin*, 2005]. However, it should be noted the corrected version of the model does not have a representation for the effects of eddy transport of O_3 across the subtropical jet. These eddy fluxes would be expected to increase O_3 in the upper tropical troposphere. The existence of an anticorrelation between O_3 and N_2O between 140 hPa and 100 hpa in the tropics suggests that some of the O_3 in this interval is of stratospheric origin [*Folkins et al.*, 1999].

[11] In the tropics, the mean CO mixing ratio is roughly constant up to 14 km. Above this height, CO diminishes in response to a decrease in convective outflow [*Folkins et al.*, 2006]. The solid black lines in Figure 3 show the seasonal cycles of tropical mean CO at 147 hPa ($\sim$14.2 km) and 100 hPa ($\sim$16.6 km) obtained from Aura Microwave Limb Sounder (MLS) measurements [*Filipiak et al.*, 2005]. The seasonal cycle at 147 hPa is probably driven by some combination of the CO seasonal cycle in the Northern Hemisphere, and by seasonal changes in tropical biomass burning. The red symbols in Figure 2 show monthly mean averages of CO interpolated to 14.2 km and 16.6 km, obtained from measurements taken between February 1, 2004 and February, 2006, by the Atmospheric Chemistry Experiment - Fourier Transform Spectrometer (ACE - FTS) [*Bernath et al.*, 2005; *Boone et al.*, 2005].

[12] The two column model was tuned to agree with the MLS monthly mean CO value at 147 hPa by setting $[CO]_{conv}$ equal to the MLS value at 147 hPa, plus 5 ppbv. The blue curves in Figure 3 show the model results at 14.2 km and 16.6 km. The uncorrected version of the model (solid line) is in reasonable agreement with observed CO mixing ratios for most of NH fall and winter (with the exception of January and February). The corrected version of the model (dashed line) is in good agreement with observed CO mixing ratios during NH summer. This pattern of agreement and disagreement is similar to that exhibited by the two model versions for O_3. The O_3 underestimate, and CO overestimate, by the corrected version of the model during NH winter may reflect the absence from the model of a representation of eddy transport, whose effects may be significantly stronger during NH winter than summer [*Waugh and Polvani*, 2000].

[13] Radiation is the dominant source of diabatic heating in the clear sky atmosphere. Air parcels which detrain above the Level of Zero radiative Heating (LZH) can be expected to have a higher probability of ascending into the stratosphere than those which detrain below the LZH. Figure 1 (middle) shows that the LZH occurs near 16.2 km in February, so that the air parcels that reach the cold point tropopause in this month ($\sim$17 km) have presumably
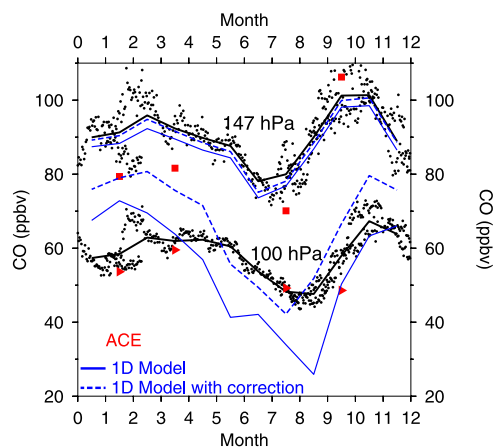

Figure 3. The solid black lines show the seasonal variation of tropical mean CO (20°S−20°N) at 147 hPa ($\sim$14.2 km) and 100 hPa ($\sim$16.6 km). These curves were generated from daily average Aura MLS CO mixing ratios in this latitudinal interval (shown as individual points). The Aura MLS measurements extend from August 2004 to February 2006, so that some monthly means are based on data from two different years. The blue lines show the seasonal cycles of CO at 14.2 km and 16.6 km generated by the one-dimensional model. The red triangles and boxes show the mean CO mixing ratio from ACE - FTS at 14.2 km and 16.6 km.

detrained between 16.2 km and 17 km. In contrast, air that reaches the tropical tropopause in August has detrained between 15.5 and 16.5 km. Given the slower vertical velocities during NH summer, one would expect a substantial seasonal variation at 17 km in the elapsed time since convective detrainment, or "age". Equation (2) can be used to estimate the age of air as a function of altitude by setting $[X]_{conv} = L = 0$, and P = 1. This gives an estimate for the age of air at 17 km of 40 days during DJF and 100 days during JJA. The correction for extratropical mass export reduces these estimates to 25 days during DJF and 70 days during JJA. Given the degree of agreement between the two models and the O_3 and CO measurements, a best estimate for the age of air at 17 km would be 40 days during DJF and 70 days during JJA. This is reasonably consistent with a 2 month estimate for the annual mean age of air near the 390 K potential temperature surface ($\sim$17.2 km), obtained by comparing in situ CO_2 mixing ratios with surface CO_2 mixing ratios at Mauna Loa (19°N) and Samoa (14°S) [*Boering et al.*, 1996]. A trajectory study using analyzed winds showed that the mean transit time from the 340 K potential temperature surface to the 400 K potential temperature surface was about 1 month, and was independent of season [*Fueglistaler et al.*, 2004]. This transit time is not directly comparable with our age of air estimates, but would appear to indicate somewhat faster dynamics than in our model.

[14] The LZH tends to be lower at locations that are closer to the equator, or characterized by more frequent deep convection. The tropical mean LZH altitudes shown in Figure 1 are therefore somewhat higher than some previous estimates [*Folkins et al.*, 1999; *Gettelman et al.*, 2004].

[15] In using (2) to solve for the trace species profiles, we set the time derivative on the left equal to zero. Given the age of air estimates at 17 km given above, this steady state assumption is reasonable during NH winter, but would not account for a 1–2 month lagged response during NH summer.

4. Seasonal Variation of the Radiative Heating Rate and Mass Flux

[16] Figure 4 (middle) shows the seasonal variation of the clear sky radiative heating rate at 17 km under various assumptions. The blue curve is the heating rate calculated using fixed annual mean O_3 and temperature at each site, but seasonally varying water vapor. The red curve shows the change in heating rate associated with the introduction of seasonally varying O_3. The green curve shows the response to introducing a seasonal variation in temperature. The black curve is the full heating rate calculated using the seasonal variation of all variables. The dominant contributors to the seasonal variation of Q_r at the tropical tropopause are temperature and O_3, with the contribution from O_3 opposite in sign, and half the magnitude, of the contribution from temperature.

[17] The curves in Figure 4 (bottom) show the seasonal variation of the radiative mass flux obtained from the corresponding Q_r curves in Figure 4 (middle), and the seasonal variation of σ in Figure 4 (top). The reduction in the amplitude of the seasonal cycle of ω_r in going from the green curve to the black curve demonstrates the importance of O_3 in offsetting the seasonal variation in ω_r arising from the seasonal variation of temperature and static stability.

5. Conclusion

[18] Clear sky mass fluxes have been used to show that there is a significant seasonal cycle in convective outflow near the tropical tropopause. The existence of this seasonal cycle is supported by seasonal cycles in O_3 and CO. The seasonal cycle in O_3 at 17 km is mainly driven by seasonal changes in dynamics. The seasonal cycle in CO at 100 hPa is driven by some combination of a seasonal change in dynamics and a seasonality in the troposphere. Age of air is a useful diagnostic because its seasonal variation reflects the combined effects of changes in both convective outflow and upwelling. We estimate that the age of air at 17 km varies from 40 days during NH winter to 70 days during NH summer.

[19] The seasonal cycles of O_3 and CO at the tropical tropopause should provide a useful constraint on the seasonal variation of high altitude convective outflow and stratosphere-troposphere exchange (STE) in more complex models. O_3 has an additional significance because it plays an important role in the energy budget of the tropical tropopause. The seasonal cycle in O_3 tends to reduce the radiative heating rate during NH winter. This would tend to reduce the upward mass flux into the tropical stratosphere, if not offset by an additional cooling of the tropopause region during NH winter. The seasonal cycle in O_3 at the tropical tropopause should therefore have the effect of amplifying the seasonal cycle in temperature. Future increases in sea surface temperatures can be expected to increase equivalent
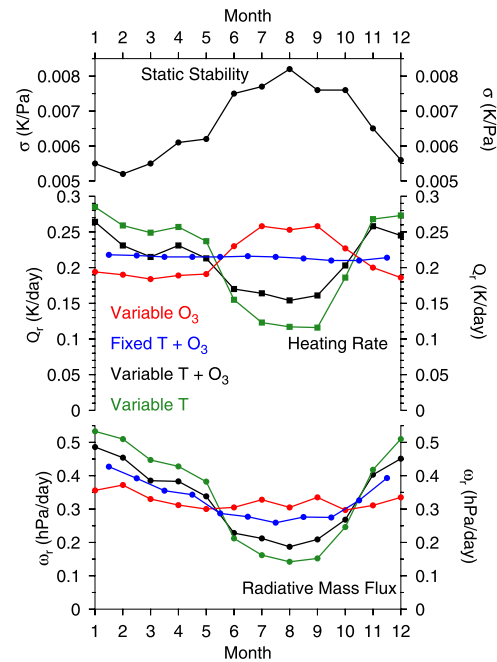

Figure 4. (top) The seasonal variation of static stability at 17 km in the tropics (20°S–20°N). (middle) Seasonal variation of the clear sky radiative heating rate at 17 km under various assumptions. (bottom) Seasonal variation of the clear sky radiative mass flux at 17 km obtained from Figure 4 (top and middle). (Upwelling rates in the lower stratosphere are often given in mm/sec. At 100 hPa, one can roughly convert from hPa/day to mm/day by multiplying by 0.63.)

potential temperatures in the tropical marine boundary layer, and may increase convective outflow near the tropical tropopause. This would contribute to a reduction in O_3 mixing ratios, and potentially, have a cooling effect on the future cold point temperatures. Recent O_3 measurements do suggest a recent increase in high altitude convective outflow [*Solomon et al.*, 2005], and it is likely that O_3 changes in the vicinity of the tropical tropopause have contributed to recent interannual variability in tropical tropopause temperatures [*Randel et al.*, 2006].

[20] The two column model used here to simulate the seasonal variation of O_3 and CO assumed that the rates of photochemical production and loss of these species had no seasonal variation. However, there is a seasonal cycle in NO_x (=NO + NO_2) at the tropical tropopause, related to seasonal variations in the convective detrainment of lightning generated NO_x near the tropical tropopause [*Park et al.*, 2004]. It is likely that the hydroxyl radical (OH) also exhibits a seasonal cycle at the tropical tropopause, due in part to seasonal cycles in water vapor, O_3, CO, and NO_x. Additional measurements of these and other O_3 precursors in the upper tropical troposphere are needed to account for these sensitivities. Further measurements are also needed to quantify the role played by STE in affecting the seasonal variation of O_3 near the tropical tropopause.

References

Bernath, P. F., et al. (2005), Atmospheric Chemistry Experiment (ACE): Mission overview, *Geophys. Res. Lett.*, *32*, L15S01, doi:10.1029/2005GL022386.

Boering, K. A., et al. (1996), Stratospheric mean ages and transport rates from observations of carbon dioxide and nitrous oxide, *Science*, *274*, 1340–1343.

Boone, C. D., et al. (2005), Retrievals for the atmospheric chemistry experiment Fourier-transform spectrometer, *Appl. Opt.*, *44*, 72187218.

Corti, T., et al. (2005), Mean radiative energy balance and vertical mass fluxes in the equatorial upper troposphere and lower stratosphere, *Geophys. Res. Lett.*, *32*, L06802, doi:10.1029/2004GL021889.

Filipiak, M. J., et al. (2005), Carbon monoxide measured by the EOS Microwave Limb Sounder on Aura: First results, *Geophys. Res. Lett.*, *32*, L14825, doi:10.1029/2005GL022765.

Folkins, I., and R. V. Martin (2005), The vertical structure of tropical convection, and its impact on the budgets of water vapor and ozone, *J. Atmos. Sci.*, *62*, 1560–1573.

Folkins, I., M. Loewenstein, J. Podolske, S. Oltmans, and M. Proffitt (1999), A barrier to vertical mixing at 14 km in the tropics: Evidence from ozonesondes and aircraft measurements, *J. Geophys. Res.*, *104*, 22,095–22,102.

Folkins, I., C. Braun, A. M. Thompson, and J. Witte (2002), Tropical ozone as an indicator of deep convection, *J. Geophys. Res.*, *107*(D13), 4184, doi:10.1029/2001JD001178.

Folkins, I., P. Bernath, C. Boone, L. J. Donner, A. Eldering, G. Lesins, R. V. Martin, B.-M. Sinnhuber, and K. Walker (2006), Testing convective parameterizations with tropical measurements of HNO$_3$, CO, H$_2$O, and O$_3$: Implications for the water vapor budget, *J. Geophys. Res.*, doi:10.1029/2006JD007325, in press.

Fu, Q., and K. N. Liou (1992), On the correlated k-distribution method for radiative transfer in nonhomogeneous atmospheres, *J. Atmos. Sci.*, *49*, 2139–2156.

Fueglistaler, S., H. Wernli, and T. Peter (2004), Tropical troposphere-to-stratosphere transport inferred from trajectory calculations, *J. Geophys. Res.*, *109*, D03108, doi:10.1029/2003JD004069.

Gettelman, A., et al. (2004), Radiation balance of the tropical tropopause layer, *J. Geophys. Res.*, *109*, D07103, doi:10.1029/2003JD004190.

Grooss, J.-U., and J. M. Russell III (2005), Technical Note: A stratospheric climatology for O$_3$, H$_2$O, CH$_4$, NO$_x$, HCl and HF derived from HALOE measurements, *Atmos. Chem. Phys.*, *5*, 2797–2807.

Logan, J. A. (1999), An analysis of ozonesonde data for the troposphere: Recommendations for testing 3-D models, and development of a gridded climatology for tropospheric ozone, *J. Geophys. Res.*, *104*, 16,115–16,149.

Park, M., W. J. Randel, D. E. Kinnison, R. R. Garcia, and W. Choi (2004), Seasonal variation of methane, water vapor and nitrogen oxides near the tropopause: Satellite observations and model simulation, *J. Geophys. Res.*, *109*, D03302, doi:10.1029/2003JD003706.

Randel, W. J., F. Wu, H. Vmel, G. E. Nedoluha, and P. Forster (2006), Decreases in stratospheric water vapor after 2001: Links to changes in the tropical tropopause and the Brewer-Dobson circulation, *J. Geophys. Res.*, *111*, D12312, doi:10.1029/2005JD006744.

Solomon, S., et al. (2005), On the distribution and variability of ozone in the tropical upper troposphere: Implications for tropical deep convection and chemical-dynamical coupling, *Geophys. Res. Lett.*, *32*, L23813, doi:10.1029/2005GL024323.

Thompson, A. M., et al. (2003a), Southern Hemisphere Additional Ozonesondes (SHADOZ) 1998–2000 tropical ozone climatology: 1. Comparison with Total Ozone Mapping Spectrometer (TOMS) and ground-based measurements, *J. Geophys. Res.*, *108*(D2), 8238, doi:10.1029/2001JD000967.

Thompson, A. M., et al. (2003b), Southern Hemisphere Additional Ozonesondes (SHADOZ) 1998–2000 tropical ozone climatology: 2. Tropospheric variability and the zonal wave-one, *J. Geophys. Res.*, *108*(D2), 8241, doi:10.1029/2002JD002241.

Waugh, D. W., and L. M. Polvani (2000), Climatology of intrusions into the tropical upper troposphere, *Geophys. Res. Lett.*, *27*, 3857–3860.

Zhang, C. (1993), On the annual cycle in highest clouds in the tropics, *J. Clim.*, *6*, 1987–1990.

————————————

P. Bernath, C. Boone, and K. Walker, Department of Chemistry, University of Waterloo, Waterloo, ON, Canada N2L 3G1.

I. Folkins and G. Lesins, Department of Physics and Atmospheric Science, Dalhousie University, Halifax, NS, Canada B3H 3J5. (ian.folkins@dal.ca)

N. Livesey, Jet Propulsion Laboratory, Pasadena, CA 91109, USA.

A. M. Thompson, Department of Meteorology, Penn State University, University Park, PA 16802-5013, USA.

J. C. Witte, Science Systems and Applications, Inc., NASA Goddard Space Flight Center, Greenbelt, MD 20770, USA.